J. Korean Soc. Ind. Appl. Math. Vol.26, No.4, 333–342, 2022 http://doi.org/10.12941/jksiam.2022.26.333

DIRECT COMPARISON STUDY OF THE CAHN–HILLIARD EQUATION WITH REAL EXPERIMENTAL DATA

DARAE JEONG [1], SEOKJUN HAM [2], AND JUNSEOK KIM[2†]

[1]DEPARTMENT OF MATHEMATICS, KANGWON NATIONAL UNIVERSITY, GANGWON-DO 24341, REPUBLIC OF KOREA

[2]DEPARTMENT OF MATHEMATICS, KOREA UNIVERSITY, SEOUL 02841, REPUBLIC OF KOREA
Email address: [†]cfdkim@korea.ac.kr

ABSTRACT. In this paper, we perform a direct comparison study of real experimental data for domain rearrangement and the Cahn–Hilliard (CH) equation on the dynamics of morphological evolution. To validate a mathematical model for physical phenomena, we take initial conditions from experimental images by using an image segmentation technique. The image segmentation algorithm is based on the Mumford–Shah functional and the Allen–Cahn (AC) equation. The segmented phase-field profile is similar to the solution of the CH equation, that is, it has hyperbolic tangent profile across interfacial transition region. We use unconditionally stable schemes to solve the governing equations. As a test problem, we take domain rearrangement of lipid bilayers. Numerical results demonstrate that comparison of the evolutions with experimental data is a good benchmark test for validating a mathematical model.

1. INTRODUCTION

A phase transition is the transformation of a thermodynamic system from one phase to another. It includes rapid behavioral change, for instance, spinodal decomposition, eutectic transformation, liquid crystal, liquid evaporation, etc. We focus on the spinodal decomposition which is the process through which a thermodynamically unstable system separates into its components which can be either two phases of the same chemical species or phases of different composition [1]. Spinodal decomposition of mixtures has been studied experimentally [2, 3, 4, 5, 6, 7, 8], mathematically [9, 10, 11, 12, 13, 14, 15, 16, 17], and numerically [18, 19, 20, 21, 22, 23, 24, 25, 26] by many researchers. Also, there have been many experimental and numerical comparison studies [27, 28, 29]. However, compared to an enormous amount of numerical simulations, there has been no direct comparison study of morphological evolution with real experimental data. To the authors' knowledge, the present study is the

Received by the editors October 18 2022; Revised December 19 2022; Accepted in revised form December 20 2022; Published online December 25 2022.

Key words and phrases. Phase transition, Spinodal decomposition, Cahn–Hilliard equation, image segmentation, phase-field method.

[†] Corresponding author.

first attempt to use the experimental configuration as an initial condition and compare the real experimental data and the simulation results from the mathematical model. Burger et al. [29] studied phase decomposition by comparing the numerical simulation and experiment results, see Fig. 1. However, the authors chose a different initial condition, which was not the same profile of the experimental data.

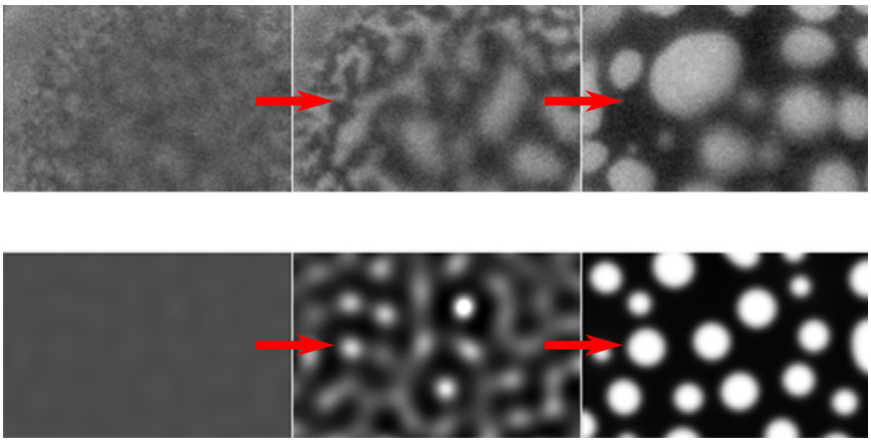

FIGURE 1. Top and bottom rows are real experiment and numerical simulation results, respectively. Reprinted from Burger et al. [29], with permission from the American Chemical Society.

The main objective of this work is, therefore, to validate a mathematical model for microstructure evolution phenomena by using the initial configuration from the real experimental data. This paper is organized as follows. In Section 2, we briefly review the Cahn–Hilliard (CH) equation. In Section 3, we describe the image segmentation technique which is based on the Mumford–Shah functional and the Allen–Cahn equation. In Section 4, we present numerical algorithms of the CH equation and image segmentation. In Section 5, we present various numerical results. Conclusions are drawn in Section 6.

2. CAHN–HILLIARD EQUATION

The Cahn–Hilliard equation is a phenomenological mathematical model of phase separation in a binary mixture [30].

$$\frac{\partial \phi(x,y,t)}{\partial t} = M\Delta\mu(x,y,t), \quad (x,y) \in \Omega,\ 0 < t \le T, \tag{2.1}$$

$$\mu(x,y,t) = F'(\phi(x,y,t)) - \epsilon^2\Delta\phi(x,y,t), \tag{2.2}$$

where M is a mobility, $F(\phi) = 0.25(\phi^2-1)^2$ is a free energy function, and ϵ is positive small constant. Typically, we use Neumann boundary conditions as

$$\mathbf{n}\cdot\nabla\phi = 0, \tag{2.3}$$

$$\mathbf{n} \cdot \nabla \mu = 0 \quad \text{on } \partial\Omega, \tag{2.4}$$

where $\mathbf{n}$ is normal to $\partial\Omega$. Equation (2.3) means the interface meets the domain boundary with 90° and Eq. (2.4) is intended for mass conservation. For more details about physical and mathematical derivations of the CH equation, see reference [31] and the references therein.

3. IMAGE SEGMENTATION ALGORITHM

To obtain the initial configuration from real experimental data, we use a recently developed image segmentation algorithm which is based on the Mumford–Shah functional and the Allen–Cahn equation [32]. The equation is given as

$$\psi_t = -\frac{F'(\psi)}{\delta^2} + \Delta\psi + \lambda[(1-\psi)(f_0 - c_2)^2 - (1+\psi)(f_0 - c_1)^2], \tag{3.1}$$

where δ is a phase transition width parameter, λ is a nonnegative parameter, and f_0 is the given image. Also, c_1 and c_2 are the averages of f_0 in the regions satisfying $\psi \geq 0$ and $\psi < 0$, respectively:

$$c_1 = \frac{\int_\Omega f_0(\mathbf{x})[1+\psi(\mathbf{x})]d\mathbf{x}}{\int_\Omega [1+\psi(\mathbf{x})]d\mathbf{x}} \text{ and } c_2 = \frac{\int_\Omega f_0(\mathbf{x})[1-\psi(\mathbf{x})]d\mathbf{x}}{\int_\Omega [1-\psi(\mathbf{x})]d\mathbf{x}}.$$

Once ψ reaches a steady state, the zero level set of ψ becomes the contour that separates the object from the background. More details about the modeling and the basic mechanism of the image segmentation algorithm can be found in reference [32].

4. NUMERICAL SOLUTION

In this section, we describe the numerical schemes for the CH equation and image segmentation algorithm.

4.1. **Numerical scheme for the Cahn–Hilliard equation.** Equations (2.1) and (2.2) are discretized in a two-dimensional space $\Omega = (a,b) \times (c,d)$. We use a $N_x \times N_y$ mesh grid, where N_x and N_y are positive even integers. $h = (b-a)/N_x$ is a space step and $\Omega_h = \{(x_i, y_j) : x_i = (i-0.5)h, y_j = (j-0.5)h, 1 \leq i \leq N_x, 1 \leq j \leq N_y\}$ is a discrete domain. Let ϕ_{ij}^n and μ_{ij}^n be approximations of $\phi(x_i, y_j, t_n)$ and $\mu(x_i, y_j, t_n)$, respectively. Here, $t_n = n\Delta t$ and Δt is a time step size. For simplicity, we take $M = 1$ as constant mobility. The CH Eqs. (2.1) and (2.2) can be discretized by using an unconditionally stable scheme as

$$\begin{aligned} \frac{\phi_{ij}^{n+1} - \phi_{ij}^n}{\Delta t} &= \Delta_d \mu_{ij}^{n+1} \\ \mu_{ij}^{n+1} &= (\phi_{ij}^{n+1})^3 - \phi_{ij}^n - \epsilon^2 \Delta_d \phi_{ij}^{n+1}. \end{aligned}$$

Here, discrete Laplacian operator is defined by $\Delta_d \phi_{ij}^{n+1} = (\phi_{i+1,j}^{n+1} + \phi_{i-1,j}^{n+1} + \phi_{i,j+1}^{n+1} + \phi_{i,j-1}^{n+1} - 4\phi_{ij}^{n+1})/h^2$. The boundary conditions (2.3) and (2.4) are discretized as

$$\begin{aligned} &\phi_{0j} = \phi_{1j},\ \phi_{N_x+1,j} = \phi_{N_x j} \text{ for } j = 1, \ldots, N_y, \\ &\phi_{i0} = \phi_{i1},\ \phi_{i,N_y+1} = \phi_{iN_y} \text{ for } i = 1, \ldots, N_x. \end{aligned}$$

For more detailed explanations, please refer to [31].

4.2. **Numerical scheme for the image segmentation.** An unconditionally stable hybrid numerical scheme for Eq. (3.1) was proposed in reference [32] as

$$\begin{aligned}\psi^{n+1,1} &= (e^{-\lambda[(f_0-c_1^n)^2+(f_0-c_2^n)^2]\Delta t}-1)\frac{(f_0-c_1^n)^2-(f_0-c_2^n)^2}{(f_0-c_1^n)^2+(f_0-c_2^n)^2} \\ &\quad + e^{-\lambda[(f_0-c_1^n)^2+(f_0-c_2^n)^2]\Delta t}\psi^n, \end{aligned} \tag{4.1}$$

$$\frac{\psi^{n+1,2}-\psi^{n+1,1}}{\Delta t} = \Delta_d \psi^{n+1,2}, \tag{4.2}$$

$$\psi^{n+1} = \psi^{n+1,2}\Big/\sqrt{e^{\frac{-2\Delta t}{\delta^2}}+(\psi^{n+1,2})^2(1-e^{\frac{-2\Delta t}{\delta^2}})}, \tag{4.3}$$

where c_1^n and c_2^n are given as

$$c_1^n = \frac{\sum_{i=1}^{N_x}\sum_{j=1}^{N_y} f_{0,ij}(1+\psi_{ij}^n)}{\sum_{i=1}^{N_x}\sum_{j=1}^{N_y}(1+\psi_{ij}^n)} \text{ and } c_2^n = \frac{\sum_{i=1}^{N_x}\sum_{j=1}^{N_y} f_{0,ij}(1-\psi_{ij}^n)}{\sum_{i=1}^{N_x}\sum_{j=1}^{N_y}(1-\psi_{ij}^n)}.$$

The solutions of Eqs. (4.1) and (4.3) are explicitly defined. Equation (4.2) is a heat equation and we apply a fast solver such as a multigrid method [33, 34, 35] to solve the equation.

5. NUMERICAL RESULTS

5.1. **Preparation of an initial condition using image segmentation.** First, we take an experimental image [6] (Fig. 2(a)), change it in a gray scaled image, f, and then normalize it, i.e.,

$$f_0 = \frac{f-f_{\min}}{f_{\max}-f_{\min}}, \tag{5.1}$$

where $f_{\max}$ and $f_{\min}$ are the maximum and the minimum values of the given image, respectively. As an initial condition for the image segmentation algorithm, we take $\psi^0 = 2f_0 - 1$. Using this initial condition, we solve Eqs. (4.1)–(4.3) for $n = 1, 2, 3, \cdots$ until the solution reaches a steady state ψ^∞ within a given tolerance. Figure 2(c) shows the temporal evolution of the image segmentation.

Note that we used a random initial condition perturbed around zero with maximum amplitude 0.2 on the computational domain $\Omega = (0,1)\times(0,1)$ to show the robustness of the image segmentation algorithm. In practice, we use $\psi^0 = 2f_0 - 1$ to speed up the computation. The last figure is the segmented image. We used the following parameters $\delta = 0.00938$, $\lambda = 9.5E4$, $h = 1/256$, and $\Delta t = 1.0E\text{-}5$. The numerical calculation is set to stop if the discrete l_2-norm of the difference between the $(n+1)^{\text{th}}$ and n^{th} solutions becomes less than a given tolerance $tol = 0.01$, i.e., $\|\psi^{n+1} - \psi^n\|_2 < tol$. Figure 2(b) is the overlapped image of the experimental data and the zero level contour of the segmented image. In general, because of the effect of λ

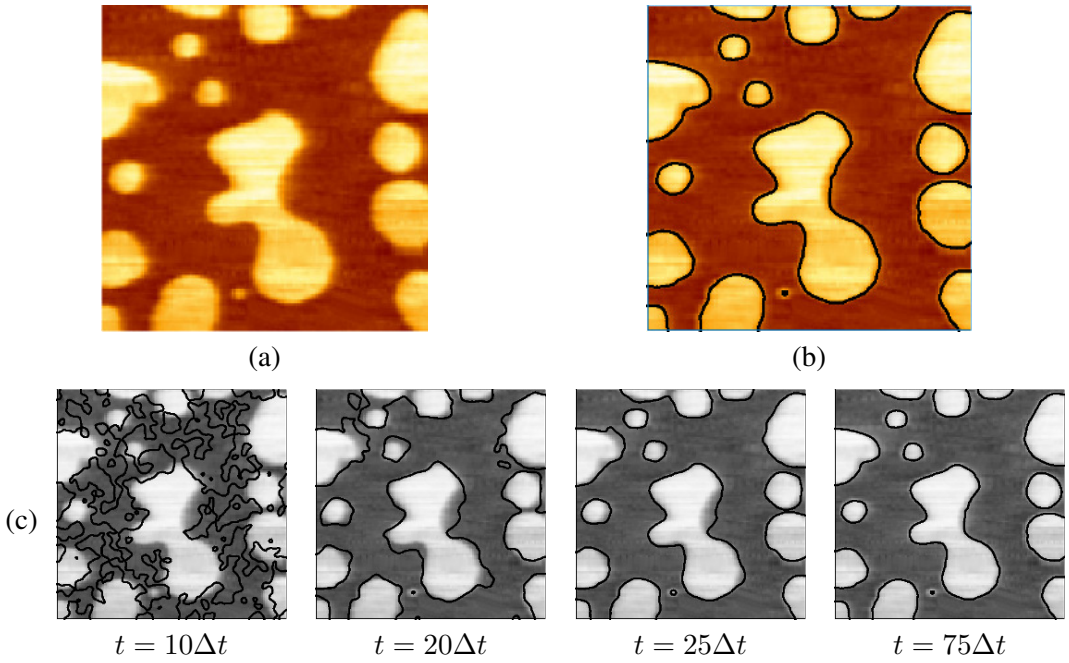

FIGURE 2. Image segmentation process to obtain initial condition for numerical experiment: (a) experimental AFM (atomic force microscope) image data, (b) overlapped image of the experimental data and the zero level contour of the segmented image, and (c) temporal evolution of the image segmentation. Reprinted with permission from [6]. Copyright ©2015. John Wiley & Sons Ltd. All rights reserved.

value, the minimum and the maximum values of $\phi^0 = \psi^\infty$ is not close to minus and plus one, respectively. Therefore, to be used as an initial condition for the CH equation, we rescale and redefine it as

$$\phi^0 = \frac{2\phi^0 - \phi^0_{\max} - \phi^0_{\min}}{\phi^0_{\max} - \phi^0_{\min}}. \tag{5.2}$$

5.2. **Numerical verification with reference data.** In this section, we numerically solve the CH equation with the segmented image as an initial condition and then, we will compare the results from the mathematical model and the real experiment. Figures 3(a) and (b) show the height images of the lipid bilayer on 14×12 micron area [6] at a reference time and after 7 minutes, respectively. In this experiment, the phase is rearranged over time as the membrane adjusts slowly to the conditions at room temperature. The small one disappears and the larger phase becomes rounded and smooth-edged. The lipid phase behavior can be modeled by the CH equation [36, 37, 38].

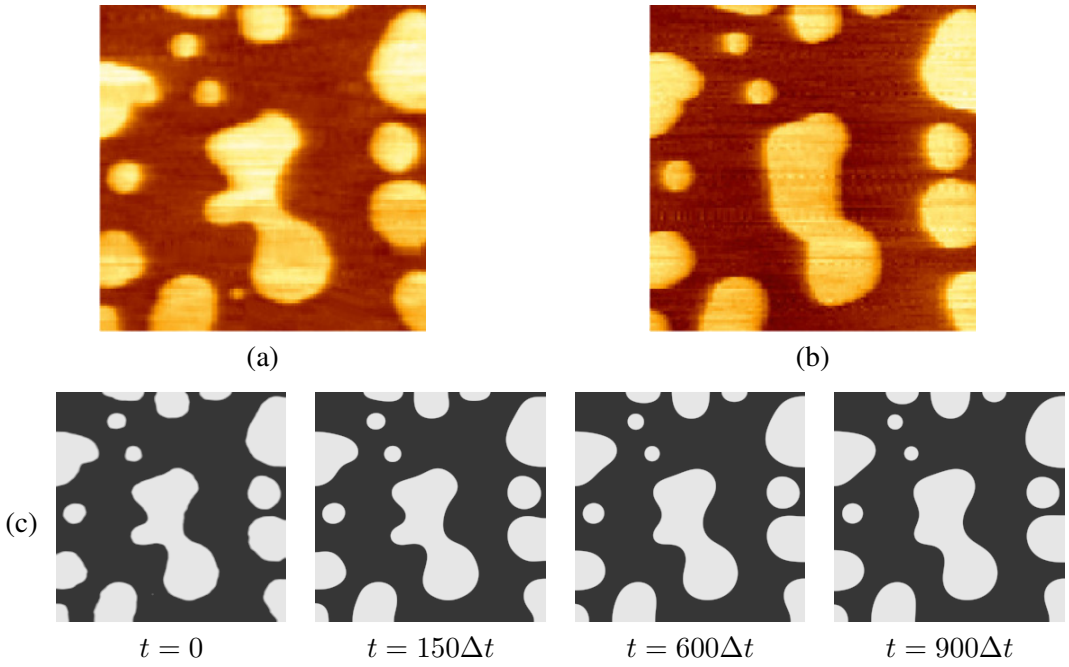

FIGURE 3. Numerical verification process with reference data which are experimental AFM (atomic force microscope) image data at (a) a reference time and (b) after 7 minutes. (c) Numerical solutions of the CH equation from $t = 0$ to $t = 900\Delta t$. Reprinted with permission from [6]. Copyright ©2015. John Wiley & Sons Ltd. All rights reserved.

Next, we numerically solve the CH equation with the segmented image (see the first image in Fig. 3(c)) on the computational domain $\Omega = (0, 1) \times (0, 1)$. We consider the interfacial transition layer parameter $\epsilon_m = mh/[2\sqrt{2}\tanh^{-1}(0.9)]$, which sets the transition layer length as mh approximately. More details about transition layer parameter are given in [39]. The parameters used are $h = 1/256$, $\epsilon = \epsilon_4$, and $\Delta t = 2h^2$. Temporal evolutions are shown in Fig. 3(c). Similar to the experimental result, we see the interface with high curvature in the center of the image becomes smoothed.

5.3. **Comparison the results of constant and variable mobility.** In this section, we compare the results of constant and variable mobility $M(\phi) = |1 - \phi^2|$. We used the parameters are as follows: spatial step size $h = 1/256$, temporal step size $\Delta t = h^2$ for constant mobility and $\Delta t = 10h^2$ for variable mobility, size of transition layer $\epsilon = \epsilon_4$ on the computational domain $(0, 1) \times (0, 1)$. Because variable mobility has an effect on the interface, it occurs the different phenomena from constant mobility as in Fig. 4 (e)–(f).

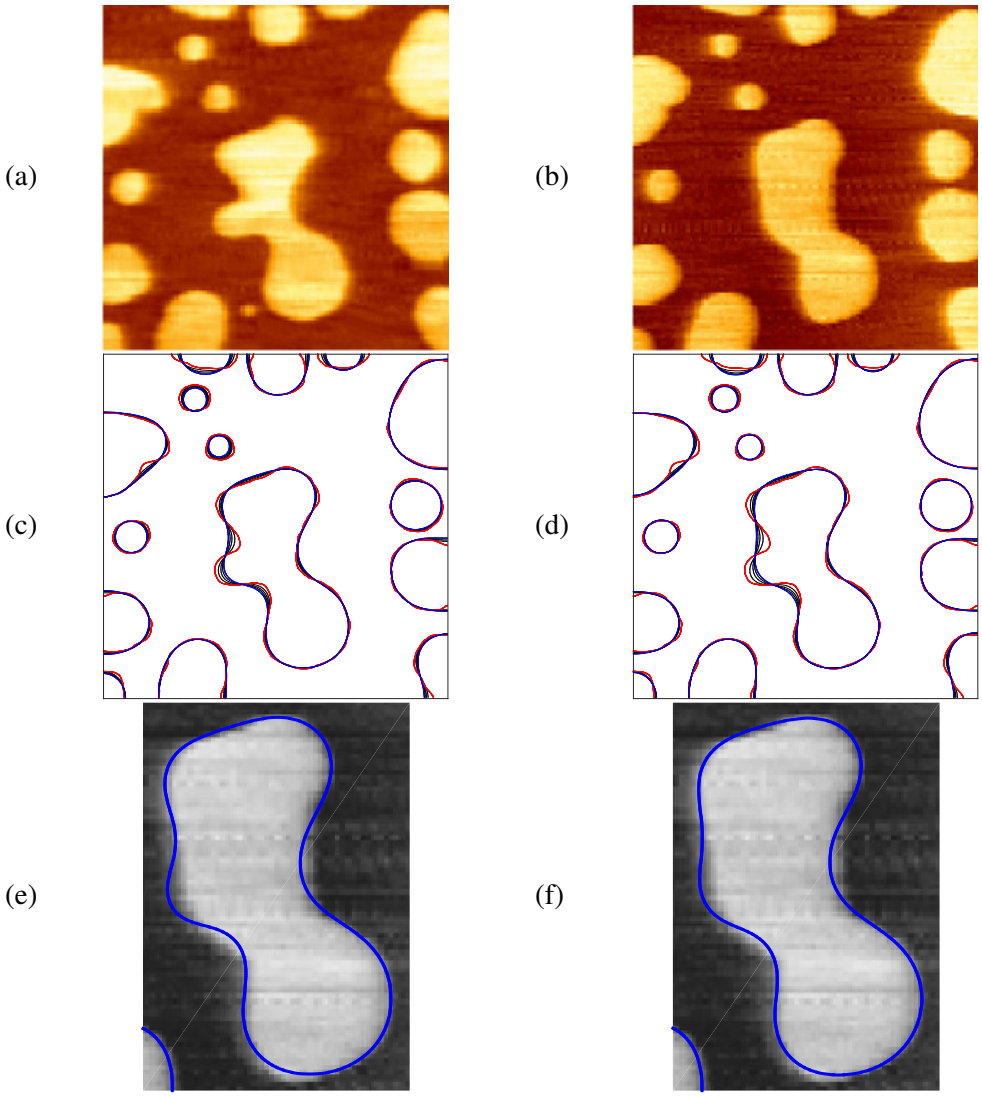

FIGURE 4. Comparison the results of constant and variable mobility. The experiment data (a) initial and (b) after evolution. (c), (d) are results by overlapping the time evolution. (c) Constant and (d) variable mobility which show the initial (red line) and final (blue line). (e) Constant and (f) variable mobility simulation results at $t = 2000\Delta t$.

6. CONCLUSION

In this paper, we proposed a method to validate a mathematical model for physical phenomena. This is done through a direct comparison study of real experimental data for domain

rearrangement and the CH equation on the dynamics of morphological evolution. With regard to the verification, we start with taking initial conditions from experimental image by an image segmentation technique. Applying the image segmentation algorithm based on the Mumford–Shah functional and the Allen–Cahn equation, we obtained the segmented phase-filed profile which is similar to the solution of the CH equation. And then, we numerically solved the CH equation with unconditionally stable scheme. As a test problem, we considered domain rearrangement of lipid bilayers. The numerical results showed good agreement in terms of morphology and interface location compared to the image data from real experimental evolution. The methodology developed in this paper suggests a numerical method for validating a mathematical equation modelling physical phenomena.

ACKNOWLEDGMENTS

The first author (D. Jeong) was supported by the National Research Foundation of Korea (NRF) grant funded by the Korea government (MSIP) (NRF-2020R1F1A1A01075937). The corresponding author (J.S. Kim) was supported by the National Research Foundation(NRF), Korea, under project BK21 FOUR. The authors appreciate the reviewers for the valuable comments on the revision of this article.

REFERENCES

[1] E. D. Siggia, *Late stages of spinodal decomposition in binary mixtures*, Physical review A, **20**(2) (1979), 595.
[2] J. T. Cabral, J. S. Higgins, T. C. B. McLeish, S. Strausser, S. N. Magonov Bulk, *spinodal decomposition studied by atomic force microscopy and light scattering*, Macromolecules, **34**(11) (2001), 3748–3756.
[3] H. J. Chung, R. J. Composto, *Breakdown of dynamic scaling in thin film binary liquids undergoing phase separation*, Physical review letters, **92**(18) (2004), 185704.
[4] B. P. Lee, J. F. Douglas, S. C. Glotzer, *Filler-induced composition waves in phase-separating polymer blends*, Physical Review E, **60**(5) (1999), 5812.
[5] F. A. Castro, C. F. Graeff, J. Heier, R. Hany, *Interface morphology snapshots of vertically segregated thin films of semiconducting polymer/polystyrene blends*, Polymer, **48**(8) (2007), 2380–02386.
[6] P. Sphingomyelin, *Lipid Rafts: Phase Separation in Lipid Bilayers studied with Atomic Force Microscopy*, https://analyticalscience.wiley.com/do/10.1002/micro.162/full/
[7] R. Blossey, *Thin film rupture and polymer flow*, Physical Chemistry Chemical Physics, **10**(34) (2008), 5177–5183.
[8] J. L. Masson, R. Limary, P. F. Green, *Pattern formation and evolution in diblock copolymer thin films above the order–disorder transition*, The Journal of Chemical Physics, **114**(24) (2001), 10963–10967.
[9] A. Novick-Cohen, L. A. Segel, *Nonlinear aspects of the Cahn-Hilliard equation*, Physica D: Nonlinear Phenomena, **10**(3) (1984), 277-298.
[10] C. M. Elliott, Z. Songmu, *On the cahn-hilliard equation*, Archive for Rational Mechanics and Analysis, **96**(4) (1986), 339-357.
[11] L. A. Caffarelli, N. E. Muler, *An L^∞ bound for solutions of the Cahn-Hilliard equation*, Archive for rational mechanics and analysis, **133**(2) (1995), 129–144.
[12] Y. Jingxue, *On the existence of nonnegative continuous solutions of the Cahn-Hilliard equation*, Journal of differential equations, **97**(2) (1992), 310–327.
[13] C. M. Elliott, H. Garcke, *On the Cahn–Hilliard equation with degenerate mobility*, Siam journal on mathematical analysis, **27**(2) (1996), 404-423.

[14] P. C. Fife, *Dynamical aspects of the Cahn–Hilliard equations*, University of Tennessee; Knoxville; TN; Barret Lectures, 1991.
[15] P. C. Fife, *Models for phase separation and their mathematics*, Electron. J. Differ. Eq. Conf., **48** (2000), 1–26.
[16] M. Grinfeld, A. Novick-Cohen, *Counting stationary solutions of the Cahn–Hilliard equation by transversality arguments*, Proceedings of the Royal Society of Edinburgh Section A: Mathematics, **125**(2) (1995), 351–370.
[17] P. Rybka, K. H. Hoffnlann, *Convergence of solutions to Cahn-Hilliard equation*, Communications in partial differential equations, **24**(5–6) (1999), 1055–1077.
[18] D. Furihata, *A stable and conservative finite difference scheme for the Cahn-Hilliard equation*, Numerische Mathematik, **87**(4) (2001), 675–699.
[19] Y. He, Y. Liu, T. Tang, *On large time-stepping methods for the Cahn–Hilliard equation*, Applied Numerical Mathematics, **57**(5-7) (2007), 616-628.
[20] J. Zhu, L. Q. Chen, J. Shen, V. Tikare, *Coarsening kinetics from a variable-mobility Cahn-Hilliard equation: Application of a semi-implicit Fourier spectral method*, Physical Review E, **60**(4) (1999), 3564.
[21] E. V. L. De Mello, O. T. da Silveira Filho, *Numerical study of the Cahn–Hilliard equation in one, two and three dimensions*, Physica A: Statistical Mechanics and its Applications, **347** (2005), 429–443.
[22] M. I. M. Copetti, C. M. Elliott, *Numerical analysis of the Cahn-Hilliard equation with a logarithmic free energy*, Numerische Mathematik, **63Z**(1) (1992), 39–65.
[23] T. M. Rogers, R. C. Desai, *Numerical study of late-stage coarsening for off-critical quenches in the Cahn-Hilliard equation of phase separation*, Physical Review B, **39**(16) (1989), 11956.
[24] C. M. Elliott, D. A. French, *Numerical studies of the Cahn-Hilliard equation for phase separation, IMA Journal of Applied Mathematics*, **38**(2) (1987), 97–128.
[25] L. Ju, J. Zhang, Q. Du, *Fast and accurate algorithms for simulating coarsening dynamics of Cahn–Hilliard equations, Computational Materials Science*, **108**(2015), 272–282.
[26] Y. Zhao, P. Stein, B. X. Xu, *Isogeometric analysis of mechanically coupled Cahn–Hilliard phase segregation in hyperelastic electrodes of Li-ion batteries*, Computer Methods in Applied Mechanics and Engineering, **297**, 325–347.
[27] Y. Shang, L. Fang, M. Wei, C. Barry, J. Mead, D. Kazmer, *Verification of numerical simulation of the self-assembly of polymer-polymer-solvent ternary blends on a heterogeneously functionalized substrate*, Polymer, **52**(6) (2011), 1447–1457.
[28] H. Mantz, K. Jacobs, K. Mecke, *Utilizing Minkowski functionals for image analysis: a marching square algorithm*, Journal of Statistical Mechanics: Theory and Experiment, **2008**(12) (2008), 12015.
[29] S. Burger, T. Fraunholz, C. Leirer, R. H. Hoppe, A. Wixforth, M. A. Peter, T. Franke, *Comparative study of the dynamics of lipid membrane phase decomposition in experiment and simulation*, Langmuir, **29**(25) (2013), 7565–7570.
[30] J. W. Cahn, *On spinodal decomposition*, Acta metallurgica, **9**(9) (1961), 795–801.
[31] D. Lee, J. Y. Huh, D. Jeong, J. Shin, A. Yun, J. Kim, *Physical, mathematical, and numerical derivations of the Cahn–Hilliard equation*, Computational Materials Science, **81** (2014), 216–225.
[32] Y. Li, J. Kim, *An unconditionally stable hybrid method for image segmentation*, Applied Numerical Mathematics, **82** (2014), 32–43.
[33] W. L. Briggs, *A Multigrid Tutorial*, SIAM, Philadelphia, 1987.
[34] U. Trottenberg, C. Oosterlee, A. Schüller, *Multigrid*, Academic Press, London, 2001.
[35] M. Donatelli, C. Garoni, C. Manni, S. Serra-Capizzano, H. Speleers, *Robust and optimal multi-iterative techniques for IgA collocation linear systems*, Computer Methods in Applied Mechanics and Engineering, **284** (2015), 1120–1146.
[36] H. K. Kodali, B. Ganapathysubramanian, *A computational framework to investigate charge transport in heterogeneous organic photovoltaic devices*, Computer Methods in Applied Mechanics and Engineering, **247** (2012), 113–129.
[37] Y. G. Smirnova, M. Fuhrmans, I. A. B. Vidal, M. Muller, *Free-energy calculation methods for collective phenomena in membranes*, Journal of Physics D: Applied Physics, **48**(34) (2015), 343001.

[38] J. Fan, T. Han, M. Haataja, *Hydrodynamic effects on spinodal decomposition kinetics in planar lipid bilayer membranes*, The Journal of Chemical Physics, **133**(23) (2010), 235101.
[39] J. W. Choi, H. G. Lee, D. Jeong, J. Kim, *An unconditionally gradient stable numerical method for solving the Allen–Cahn equation*, Physica A, 388(9) (2009), 1791–1803.